Efficient MoM Simulation of 3-D Antennas in the Vicinity of the Ground

Khaldoun Alkhalifeh, *Member, IEEE*, Greg Hislop, *Senior Member, IEEE*, Nilufer Aslihan Ozdemir, *Member, IEEE*, and Christophe Craeye, *Senior Member, IEEE*

***Abstract*— A novel fast technique is presented to account for the effect of an arbitrary soil permittivity in the analysis of ground penetrating radar antennas in the presence of a flat layered ground. We named the method fast ground coupling matrix because it is expressed as an additional method-of-moment (MoM) impedance matrix obtained from the radiation patterns of the basis/testing functions and the ground reflection coefficient. The advantage of this method is the independence of radiation patterns from the ground's physical and electromagnetic parameters (layer thickness, complex permittivity, permeability, and so on). The new matrix formulation efficiently calculates the impedance matrix due to the ground's contribution, with a loop over the ground parameters (permittivity, conductivity, and/or permeability), and changing the distance between antenna and ground. The number of samples in (complex) spectral domain is dramatically reduced by explicitly compensating truncation with aliasing errors in the spectral integration. To demonstrate the accuracy and efficiency of the proposed method, numerical results for 3-D metallic Vivaldi and typical dipole antennas are presented. Good agreement among the exact MoM solutions, the simulation results, and measured data is observed over an ultrawide bandwidth.**

***Index Terms*— Conductivity, contour deformation, dielectric measurements, Green's function, ground penetration radar (GPR), method of moments (MoM), permittivity, ultrawideband.**

I. Introduction

GROUND-PENETRATING radar (GPR) is currently the subject of intensive research for various applications such as investigation of soil, e.g., for agriculture [1], [2], road pavement verification [3], [4], water leak detection [5], [6], and ground dielectric permittivity estimation [7]–[10]. For such applications, the antenna is very close to an object, such as the lossy ground, which will strongly modify the antenna input impedance [11] and radiated near-fields. Such applications require the antenna(s) to be intensively simulated for a wide range of ground types (permittivity, conductivity, permeability, multilayered medium, and so on). Such simulations may help identifying the best antenna type for given average ground properties. When the layered-medium corresponds to an acceptable approximation below the antenna footprint, such simulations may also assist the estimation of the layers properties. Indeed, the active antenna will be expected to collect data from a large number of prospective ground types with various parameters. Structures composed of a radiator and a layered medium can be analyzed via full-wave frequency-domain integral equation techniques discretized and solved using the method of moments (MoM) [12]. The surface integral equation (SIE) approach has been used for the analysis of antennas [13], [14], where the dyadic Green's function for Layered Media is employed to take into account the effect of the dielectric material [15]–[18]. Chen *et al.* [19] used a method based on the hybrid volume-SIE. The modeling of antennas and medium together has been investigated by different authors. Cui and Chew [20] developed an accurate model for wire antennas, above or inside the ground, using Galerkin testing. A 3-D model based on the finite-difference time-domain (FDTD) method has been developed by Giannopoulos [21] (GPRMax) to simulate GPR antennas in the presence of dielectric material.

A new method, named fast ground coupling matrix (FGCM) is proposed here to account for the interaction between antennas and a ground composed of arbitrary layers. In this paper, 3-D metallic antennas are chosen as examples. The FGCM method relies on the MoM solution of SIEs to solve the electromagnetic problem that involves metallic antennas radiating above a planar, possibly layered, ground. The proposed method starts by separating the MoM matrix into two terms: a free-space matrix Z^f and a matrix Z^g that accounts for the presence of the ground. Such separation can be found in [20] in the case of flat substrates, and in [22] for cylindrical substrates. The free-space matrix is calculated using the brute-force MoM approach; it can be efficiently interpolated versus frequency using the FMIR -MoM [23]. The ground reflection matrix Z^g is calculated as a product of radiation patterns of the basis functions (BFs)/testing functions (TFs) with the ground's reflection coefficient, integrated following a specific path along the complex spectral coordinates (k_x, k_y). Here, the steepest-descent path (SDP) [24] is considered. The radiation patterns of the BFs/TFs depend on the (k_x, k_y) coordinates. A grid with a minimal number of points is achieved by explicitly compensating aliasing and truncation errors, as done in [25] in the 2-D case. The independence of the ground physical and electromagnetic parameters when generating the radiation patterns allows the efficient calculation of the MoM impedance matrix

Manuscript received February 26, 2016; revised July 28, 2016; accepted September 27, 2016. Date of publication October 19, 2016; date of current version December 5, 2016. This work was supported by the SENSPORT Project of Region Wallone.

K. Alkhalifeh and C. Craeye are with Institute of Information and Communication Technologies, Electronics and Applied Mathematics, Université catholique de Louvain, Louvain-la-Neuve 1348, Belgium (e-mail: khaldoun.alkhalifeh@uclouvain.be; christophe.craeye@uclouvain.be).

G. Hislop is with Fugro Roames, Brisbane 4113, QLD, Australia (e-mail: gregory.hislop@gmail.com).

N. A. Ozdemir is with the Royal Observatory of Belgium, Uccle 1180, Belgium (e-mail: nilufer.ozdemir@oma.be).

Color versions of one or more of the figures in this paper are available online at http://ieeexplore.ieee.org.

Digital Object Identifier 10.1109/TAP.2016.2618482

that describes the coupling between antenna and ground. The operations needed to update the MoM impedance matrix after changing the ground parameters consists of uploading the offline free-space matrix Z^f and offline BFs/TFs radiation patterns, and performing the efficient calculation of the reflection coefficient versus (k_x, k_y). The latter two operations allow the fast calculation of the ground coupling impedance matrix Z^g. Following [25], the number of points in the (k_x, k_y) plane is strongly reduced based on a systematic compensation between aliasing and truncation errors. The significant advantage of this technique is that it only needs once the calculation of Z^f and of the radiation patterns of the BFs/TFs once, and then a very efficient calculation of the MoM impedance matrix is achieved for given ground parameters. The FGCM method is able to simulate the antenna response for any soil parameters (permittivity, conductivity, permeability, and so on), including multilayered media. The MoM impedance matrix is also efficiently updated when changing the vertical distance between the antenna and the ground by multiplying the reflection coefficient with a factor. A limitation of this method is that it requires the antenna to be entirely above the ground. Also, the FGCM method does not speed up the matrix solution step, which could be done using the macro BF approach [26], [27]. Preliminary simulation results of the proposed method are reported in [28], while this paper presents full details of the method, as well as validations using FDTD simulation and measurements.

The remainder of this paper is organized as follows. Section II presents the detailed mathematical formulation of the FGCM method. In Section III, numerical results obtained employing the FGCM method are validated with respect to the brute-force MoM approach, IE3D and SEMCAD commercial software. The computation times for the proposed method are also reported in this section. In Section IV, the obtained numerical results are validated with respect to measurements and the performance of the method is discussed. Finally, conclusions are drawn in Section V.

II. Mathematical Formulation

A. TE and TM Waves

Consider sources above a mutilayered medium, excited by known electric and magnetic currents, as illustrated in Fig. 1. The fields above $z = 0$ can be decomposed into TE and TM plane waves associated with spectral coordinates (k_x, k_y). Those plane waves are expressed as follows:

$$\vec{E} = (-\hat{m}\, A_{TE} + \hat{e}\, A_{TM})\, e^{-jk_x x}\, e^{-jk_y y}\, e^{\pm jk_z z} \tag{1}$$

$$\vec{H} = \frac{1}{\eta}\, (\hat{e}\, A_{TE} + \hat{m}\, A_{TM}) e^{-jk_x x}\, e^{-jk_y y}\, e^{\pm jk_z z} \tag{2}$$

where in the exponent along z, the $\mp$ sign corresponds to electromagnetic waves propagating in the $\pm z$-direction, and A is the complex amplitude of the plane wave. The free-space impedance is denoted by η. For a given spectral component (k_x, k_y), with magnitude $\beta = (k_x^2 + k_y^2)$, propagation takes place in direction $\vec{k} = (k_x, k_y, \mp k_z)$ with

$$k_x^2 + k_y^2 + k_z^2 = k^2 = \omega^2 \epsilon_i\, \mu_i \tag{3}$$

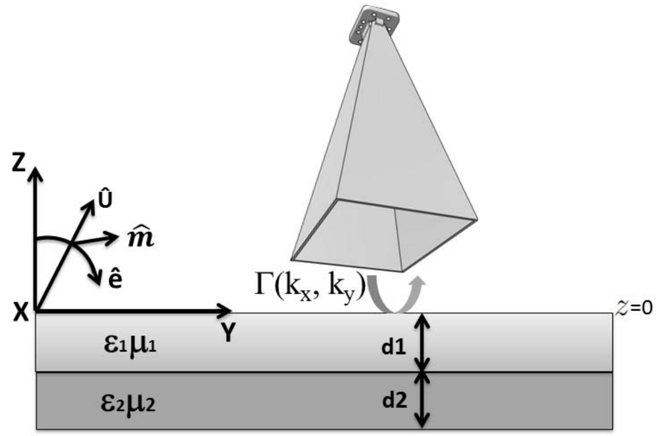

Fig. 1. Coordinates of a radiator above a multilayered medium.

where ϵ_i and μ_i are the permittivity and permeability of the ith layer in the medium [29]. The normalized direction of propagation is $\hat{u} = \vec{k}/k$. In each medium, horizontal and vertical polarization vectors are defined by vectors perpendicular to the direction of propagation for waves propagating in $+z$-direction

$$\hat{m} = \frac{1}{\beta}\begin{bmatrix} -k_y \\ k_x \\ 0 \end{bmatrix} \quad \text{and} \quad \hat{e}^u = \frac{1}{\beta\, k}\begin{bmatrix} k_x\, k_z \\ k_y\, k_z \\ -\beta^2 \end{bmatrix}. \tag{4}$$

For waves propagating in $-z$-direction

$$\hat{m} = \frac{1}{\beta}\begin{bmatrix} -k_y \\ k_x \\ 0 \end{bmatrix} \quad \text{and} \quad \hat{e}^d = \frac{1}{\beta\, k}\begin{bmatrix} -k_x\, k_z \\ -k_y\, k_z \\ -\beta^2 \end{bmatrix}. \tag{5}$$

In the TM case, $\hat{e}_p$ is $\hat{e}^u$ or $\hat{e}^d$ (upward and downward, respectively); and in the TE case, $\hat{e}_p$ is $-\hat{m}$.

B. Electromagnetic Fields Reflected From Ground

Consider the case of a 3-D antenna discretized with BFs and TFs. We split the interaction $Z = Z^f + Z^g$ between these BFs and TFs into a free-space part and a ground-reflected part. A plane-wave spectrum approach with regular (k_x, k_y) spacing [30]–[32] is used to accelerate the calculation of the ground-reflected part. Green's function reads as the Weyl integral [33]

$$\begin{aligned} G(R) &= \frac{e^{-jkR}}{4\,\pi\, R} \\ &= \frac{1}{(2\,\pi)^2} \iint_{-\infty}^{+\infty} \frac{e^{-j\,(k_x\,(x-x')+k_y\,(y-y')+k_z\,|z-z'|)}}{2\,j\,k_z} dk_x dk_y \end{aligned} \tag{6}$$

where $\vec{r}\,' = (x', y', z')$ represents the source point coordinates, $\vec{r} = (x, y, z)$ represents the observation point coordinates, and $R = \| \vec{r} - \vec{r}\,' \|$.

The vector potential in free space due to electric current density $\vec{J}_b$associated with a BF can be expressed as

$$\vec{A}(x,\ y,\ z) = \iiint_V G(R)\ \vec{J}_b(x',\ y',\ z')\ dV \tag{7}$$

In (6), the integral over (k_x, k_y) coordinates corresponds to the spectral representation of Green's function. For waves propagating in $-z$-direction, $|z-z'|$ can be rewritten as $z'-z$, such that $e^{-jk|z-z'|} = e^{jkz'}e^{-jkz}$ becomes separable. This paper assumes that the antenna is entirely above the ground in order to calculate the ground's reflection component by simply multiplying the waves propagating in $-z$-direction by the ground's reflection coefficient. The relation between the electric field intensity with p polarization (either TE or TM) and the radiated vector potential is defined as

$$\begin{aligned} E_p &= \vec{E} \cdot \hat{e}_p \\ &= -jk\eta \left(\vec{A} + \frac{\nabla\nabla\cdot\vec{A}}{k^2}\right) \cdot \hat{e}_p \\ &= \frac{-j\,k\,\eta}{(2\,\pi)^2} \iint_{k_x,k_y} \frac{e^{-j\,(k_x\,x+k_y\,y-k_z\,z)}}{2\,jk_z}\,\hat{e}_p \\ &\cdot \left\{\mathcal{I} - \frac{\bar{k}\bar{k}.}{k^2}\right\} \iiint \vec{J}_b\, e^{-j\,(k_x\,x'+k_y\,y'+k_z\,z')}\, dV \quad dk_x\, dk_y \end{aligned} \tag{8}$$

where integrations over spectral and spatial coordinates appearing in (6) and (7) have been swapped, and $\mathcal{I}$ is the identity operator. The electric field propagating in $-z$-direction $(z < z')$ with p polarization then becomes

$$E_p(x,y,z) = \frac{-j\,k\,\eta}{(2\,\pi)^2} \iint F_{b,p}(k_x,k_y) \times \frac{e^{-j\,(k_x\,x+k_y\,y-k_z\,z)}}{2\,j\,k_z}\,dk_x\,dk_y \tag{9}$$

where $F_{b,p}$ is the pattern of the corresponding BF with p polarization; it is given by

$$F_{b,p}(k_x,k_y) = \iiint_V \vec{J}_b(x',y',z')\cdot\hat{e}_p\; e^{j\,(k_x\,x'+k_y\,y'-k_z\,z')}dV. \tag{10}$$

The field reflected by the ground in the same polarization then becomes

$$E_p(x,\ y,\ z) = \frac{-j\,k\,\eta}{(2\,\pi)^2} \iint \Gamma_p(k_x,\ k_y)F_{b,p}(k_x,\ k_y) \times \frac{e^{-j\,(k_x\,x+k_y\,y-k_z\,z)}}{2\,j\,k_z}\,dk_x\,dk_y \tag{11}$$

where Γ_p is the reflection coefficient for p polarization.

The electric field tested by function $\vec{J}_t$ reads

$$I = \iiint E_p\;\hat{e}_p \cdot \vec{J}_t\; dV. \tag{12}$$

Following a procedure similar to that used in (9), I can be detailed as

$$I = \frac{-j\,k\,\eta}{(2\,\pi)^2} \iint F_{b,p}(k_x,\ k_y)F_{t,p}(k_x,\ k_y)\,\frac{1}{2\,j\,k_z} \times \Gamma_p(k_x,\ k_y)\,dk_x\,dk_y \tag{13}$$

where the radiation pattern of the TF has a slightly different form compared to that of the radiation pattern of the BF in (10)

$$F_{t,p}(k_x,\ k_y) = \iiint_V \vec{J}_t(x',y',z')\cdot\hat{e}_p\; e^{-j\,(k_x\,x'+k_y\,y'+k_z\,z')}dV \tag{14}$$

where it is important to note the changes of sign in the exponent, compared with the expression (9) of $F_{b,p}$. Regarding propagation in $+z$- versus $-z$-directions, one has to pay attention to the change in definitions of the polarization vector: x and y components of vector $\hat{e}$ change sign in the TM case [see (4) and (5)]. Hence, four different radiation patterns will be needed for this method as follows: for each BF, the radiation patterns will be calculated for TE and TM modes and for both propagation directions ($-z$ and $+z$). We also calculate the reflection coefficients Γ_{TE} and Γ_{TM} to account for the reflection from the ground.

For the results below, the SDP contour deformation is used in the complex β plane. Other types of contours, such as the parabolic contour, have been used in [34] where the impedance matrix is filled similar to Z^g. The imaginary part of β in the SDP contour deformation is defined in terms of the real part of β (β_R) as follows [25]:

$$\beta_I = \frac{\beta_R}{S} \tag{15}$$

with $S = (1 + (\beta_R/k)^2)^{1/2}$, and

$$\frac{d\beta_I}{d\beta_R} = \frac{1}{S^3} \tag{16}$$

also

$$\frac{k_{xI}}{k_{xR}} = \frac{k_{yI}}{k_{yR}} = \frac{\beta_I}{\beta_R} \tag{17}$$

with $k_x = k_{xR} + jk_{xI}$ and $k_y = k_{yR} + jk_{yI}$

For details on how (15)–(17) are obtained, one may refer to [25] and [35].

To avoid a singular integrand, we adopt a contour deformation in complex β plane with

$$\beta = \beta_R + j\beta_I = \sqrt{k_x^2 + k_y^2}. \tag{18}$$

As proven in [35], the contour deformation can be applied while still integrating over real (k_x, k_y) coordinates. To do this, it is necessary to include the following Q factor [35] in the integrand:

$$Q(k_x,k_y) = \left(1 + j\frac{d\beta_I}{d\beta_R}\right)\left(1 + j\frac{\beta_I}{\beta_R}\right) \tag{19}$$

where $\beta_I(\beta_R)$ is the function that defines the integration path.

Finally, from (13) and (19), the total tested field for a given pair (t, b) of TFs and BFs is obtained as

$$Z^g_{t,b} = \frac{-j\,k\,\eta}{(2\,\pi)^2} \iint (F_{b,TE}\,F_{t,TE}\,\Gamma_{TE} + F_{b,TM}\,F_{t,TM}\,\Gamma_{TM}) \times \frac{1}{2\,j\,k_z}\,Q(k_{xR},k_{yR})\,dk_{xR}\,dk_{yR}. \tag{20}$$

C. Spectral Sampling of (k_x, k_y) Grid Points

The spectral-domain MoM approach is employed to compute the interactions between elementary BFs and TFs. The interactions between elementary BFs can be expressed as an extension of what is found in (20).

A square grid in $(k_{xR},\ k_{yR})$ coordinates is used with $N = N_x = N_y$ points. It is important to wisely choose the density and extent of the k_{xR}, k_{xR} grid.

TABLE I
NUMBER OF INTEGRATION POINTS AND ASSOCIATED DOMAIN OF INTEGRATION

Range	nb. integ. points	The normalized integration domain k_{max}/σ
$0.91 < z/\lambda < 2.8$	13	1.4889
$0.5 < z/\lambda < 0.91$	15	1.3116
$0.2 < z/\lambda < 0.5$	17	1.1698
$0.1 < z/\lambda < 0.2$	21	1.0599
$0.05 < z/\lambda < 0.1$	25	0.8685
$z/\lambda < 0.05$	35	0.7574

As explained in [25] and [36], a proper choice of integration domain range and number of points $N = N_x = N_y$ can lead to a compensation between aliasing and truncation errors. Let us define the range of integration as from $-k_{\max}$ to $+k_{\max}$. Based on an intermediate-to-far field approximation, the integral can be proven to resemble the Fourier transform of a Gaussian function with standard deviation close to $\sigma = (k/(2z))^{1/2}$ [36], where k is the wavenumber and z is the distance between the bottom of the antenna and the ground. Therefore, a link can be established between the number of points N and the normalized half width of the integration domain $k_{\max}/\sigma$.

It is known that the number of required plane waves decreases with increasing distance between the antenna and the ground. For each chosen N, an appropriate range of distances is selected in order to attain the threshold of relative error in the order of 10^{-2} with respect to the exact solution of Green's function. The relative error is defined as

$$e_r = \frac{GF_{\text{ex}} - GF_{\text{FGCM}}}{GF_{\text{ex}}} \tag{21}$$

where GF_{ex} is the exact solution of Green's function, and GF_{FGCM} is Green's function obtained by the FGCM method. A perfect electrical conductor (PEC) ground is taken into consideration for this case. The lateral deviation $(\Delta x, \Delta y)$ is chosen as $(0.5, 0.5)\lambda$ to approximately account for the width of the antenna. Table I provides for each chosen $N = N_x = N_y$, the corresponding half width of the integration domain $k_{\max}/\sigma$, with the associated range of distances.

Suitable N_x, N_y values can be obtained by determining the minimum antenna height and referring to the corresponding N_x, N_y values in Table I. If the antenna lateral dimensions are significantly larger, Table I will need to be recalculated.

D. Numerical Implementation

To implement this approach, the values of Γ, Q, F_b, and F_t for each BF and TF can be arranged in matrix forms. One may define $\cdot*$ as the matrix element-by-element product, $*$ as a matrix product and $\bar{1}$ as a matrix of length equal to the number of BFs or TFs and width equal to one. The same mesh will be used for excitation, and we define M as the number of BFs. The integration in (20) can be written as a matrix multiplication as follows:

$$\begin{aligned}\bar{\bar{Z}}^g_{t,b} &= \bar{\bar{F}}_{t,TE} * (\bar{\bar{F}}_{b,TE} \cdot *(\bar{\Gamma}_{TE1} * \bar{1})) \\ &\quad + \bar{\bar{F}}_{t,TM} * (\bar{\bar{F}}_{b,TM} \cdot *(\bar{\Gamma}_{TM1} * \bar{1}))\end{aligned} \tag{22}$$

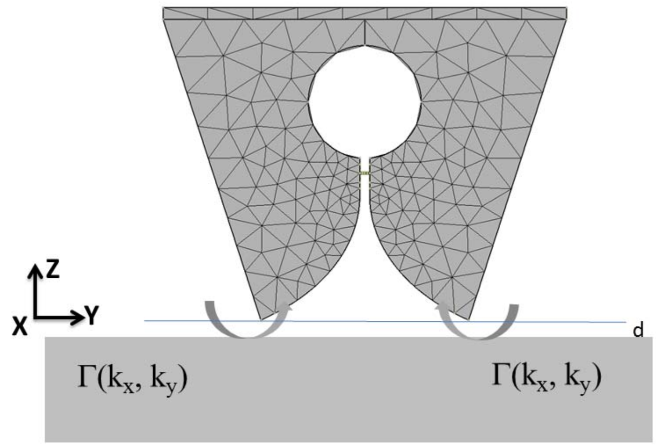

Fig. 2. Vivaldi antenna at $d = 10.75$ mm above ground.

where

$$\Gamma_{TE1} = \Gamma_{TE} \frac{-Q(k_x, k_y)}{(2\pi)^2} \frac{k\eta}{2k_z} \Delta k_x \Delta k_y$$
$$\Gamma_{TM1} = \Gamma_{TM} \frac{-Q(k_x, k_y)}{(2\pi)^2} \frac{k\eta}{2k_z} \Delta k_x \Delta k_y$$

where $\bar{\bar{F}}_{t,TE}$ is a matrix with dimensions of M by $N_x \times N_y$, $\bar{\bar{F}}_{b,TE}$ is a matrix with dimensions of $N_x \times N_y$ by M, $\bar{\Gamma}_{TE1}$, $\bar{\Gamma}_{TM1}$ are matrices with dimensions of $N_x \times N_y$ by one, and $\bar{\bar{Z}}^g_{t,b}$ is a matrix with dimensions of N_x by N_y. Δk_x and Δk_y are the wavenumber steps along k_x and k_y, respectively. When changing the ground parameters, only Γ_{TE} and Γ_{TM} need to be recomputed, and a new matrix is efficiently calculated. This sort of formulation allows for significant improvement in computational speed in certain computational languages, as MATLAB. More information about the required time to obtain the radiation patterns, reflection coefficients and to fill the matrix Z^g will be provided in Section III-A.

Then, for all pairs of BFs and TFs, the MoM impedance matrix is given by

$$Z = Z^g + Z^f \tag{23}$$

where Z^g includes all effects of interaction with the ground. Z^f is the free-space impedance matrix obtained using the brute-force MoM solution or interpolated versus frequency using FMIR-MoM [23], considering that the antenna is in free space.

III. SIMULATION RESULTS AND DISCUSSION

A. Validation Against Brute-Force MoM for a Vivaldi Antenna Above PEC Ground

The antenna under consideration is a 3-D Vivaldi antenna above a ground plane operating from 1.5 to 6 GHz. The antenna is represented by the surface mesh in Fig. 2 with 1360 RWG [37] BFs. The antenna dimensions are $7.5 \times 10 \times 0.5$ cm, and it is placed at $d = 10.75$ mm above a PEC ground, as shown in Fig. 2. The Vivaldi antenna mesh was produced using GMSH [38].

An electromagnetic simulation solver developed at UCL, based on the conventional MoM [12], was used to calculate the

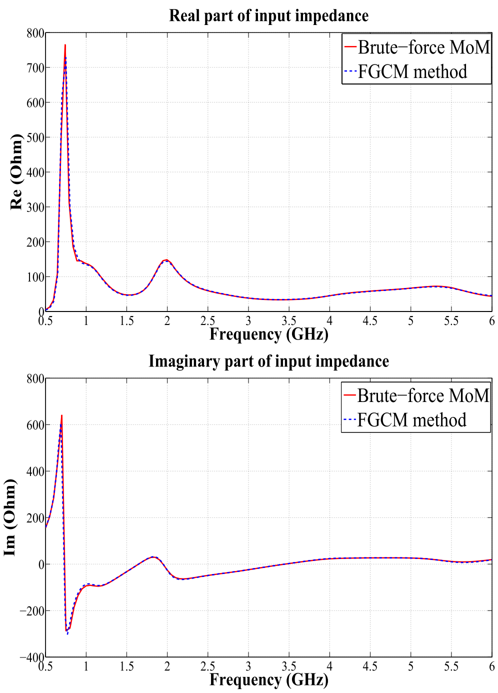

Fig. 3. Real and imaginary parts of the antenna input impedance.

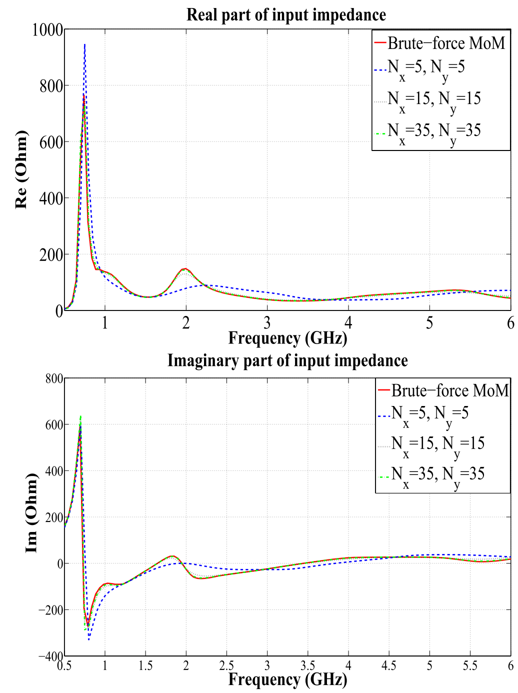

Fig. 4. Influence of (kx,ky) grid resolution.

TABLE II
FGCM DETAILED COMPUTATION TIMES

Operation	Time (s)
Free-space brute-force MoM matrix Z^f	64.3
Brute-force MoM with a PEC ground	97.8
All radiation patterns	25.5
Γ_{TE} and Γ_{TM}	0.094
Matrix multiplication and filling of Z^g	0.67
Uploading offline patterns and free-space MoM matrix	0.73

free-space impedance matrix Z^f. This software can solve the problem of an antenna in the presence of a PEC ground using image theory. It is not possible to include a dielectric ground in this example. Validations for real and imaginary parts of the input impedance can be seen in Fig. 3. The results show a very good agreement between the FGCM technique and the brute-force MoM for this type of 3-D antennas above a PEC ground.

The simulations were carried out using a PC with 24 GB RAM and a 2.4 GHz Intel Xeon Core Processor. For a single frequency, the FGCM method requires 89.9 s of preparation time, which includes the calculation of the four radiation patterns per BF, as well as the free-space brute-force MoM matrix. All matrix filling times are provided in Table II. The dimensions of the (k_x, k_y) grid are set to $N_x = N_y = 35$.

For a given set of soil parameters, it is only necessary to recalculate the reflection coefficients Γ_{TE} and Γ_{TM}, as well as the matrix multiplications in (22) after uploading the offline patterns of BFs and free-space MoM matrix. This procedure only takes 1.5 s, to be compared with 33.5 s (the difference between 97.8 and 64.3 s) in the case of brute-force MoM. It was feasible to keep the radiation pattern matrices in RAM, so we could save their uploading time. For each frequency, it is necessary to upload the radiation patterns once. The FGCM method speeds up the brute-force MoM by a factor of 22, and hence allows for efficient loops over soil parameters. The time needed to obtain the ground coupling matrix Z^g has a direct relation with the number of points in the (k_x, k_y) grid. More details on this parameter are provided in Section III-B.

B. Influence of (k_x, k_y) Grid Resolution

As explained in Section II-C, the number of points in (k_x, k_y) grid is carefully chosen based on a compensation between aliasing and truncation errors. The influence of using a coarse (k_x, k_y) grid is observed in Fig. 4, which shows the effect of different values of N_x and N_y parameters for the case of the Vivaldi antenna placed above a PEC ground. Increasing the number of points N_x, N_y from $N_x = N_y = 35$ to $N_x = N_y = 75$ will increase the time needed to create the radiation patterns from 25.5 to 115.9 s, without significant effect on accuracy.

C. Influence of the Distance Between the Antenna and the Ground

From (14) and (20), it is found that it is possible to very efficiently account for the effect of changing the vertical distance between the antenna and the ground by introducing an air layer just above the layered medium. Thus, only Γ needs to change as follows:

$$\Gamma_{TE,TM(z+\Delta z)} = \Gamma_{TE,TM(z)}\ e^{-2jk_z\Delta z} \tag{24}$$

where Δz is the difference between the two vertical distances. A simulation has been carried out applying the FGCM method for a distance of 10.75 mm between the Vivaldi antenna and

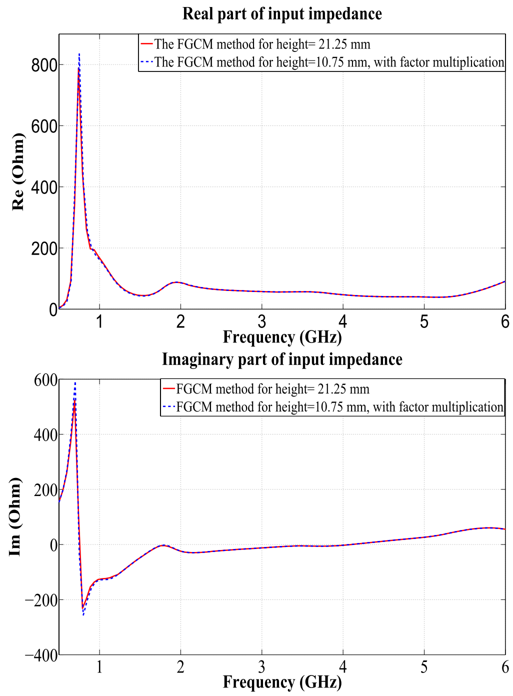

Fig. 5. Validation of antenna input impedance while modifying the vertical distance between the antenna and the ground.

TABLE III
IE3D AND FGCM COMPUTATION TIMES

Operation	Time (s)
IE3D software	0.4
FGCM method	0.156
Update of Z^g when changing ground parameters while having patterns precalculated	0.078

a PEC ground. The reflection coefficient obtained from this simulation is multiplied by the factor $e^{-2jk_z\Delta z}$, where Δz is set to 10.5 mm. The obtained results have been compared with the brute-force solution in the case of a PEC ground for a distance of 21.25 mm between the antenna and the ground. The results are in excellent accordance, as shown in Fig. 5. For comparison, the computational time needed to create the radiation patterns for a height of 21.25 mm at a single frequency is 25.5 s, while only 1.28 s are needed to update the MoM matrix by phase shifting Γ.

D. Validation Against IE3D for a Dipole Antenna Above a Multilayered Medium

The FGCM method is validated below with results obtained with the commercial software IE3D [39], while considering a dielectric ground. A horizontal dipole in the form of a 5×0.25 cm rectangular strip is placed 1 cm above a lossless multilayered medium (see Fig. 6 for medium details). For the FGCM results, the dipole is discretized using the GMSH software into 37 RWG BFs. The number of (k_x, k_y) grid points is taken as $N_x = N_y = 19$. Table III gives the computation times for both cases.

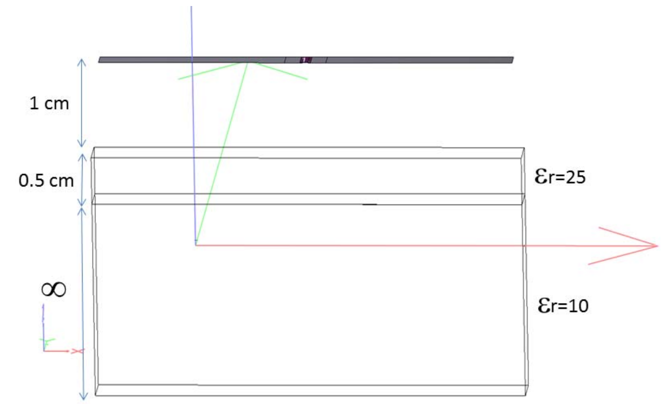

Fig. 6. Horizontal dipole in the presence of a lossless multilayered infinite ground; plot generated with IE3D.

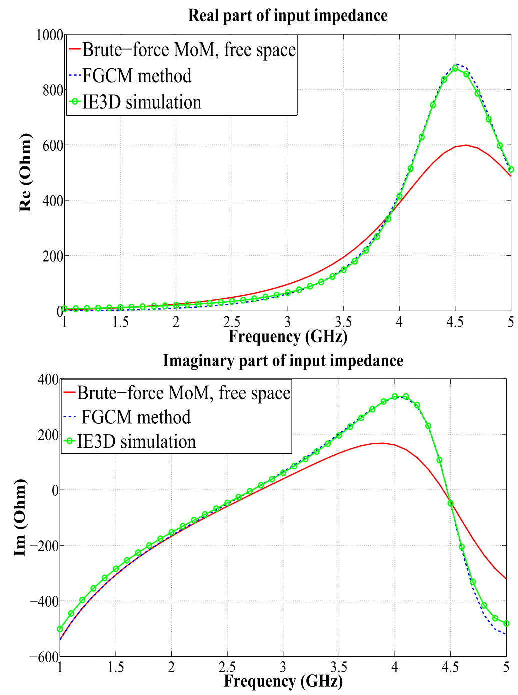

Fig. 7. Antenna real and imaginary parts of input impedance as a function of frequency for three different simulations: free-space, FGCM method, and IE3D simulation (the latter two in presence of layered medium).

Fig. 7 shows a very good agreement between the FGCM results and IE3D simulations. The free-space results added on the plots illustrate the very significant effect of the multilayered medium on the input impedance of the antenna.

E. Validation Against FDTD Method for a Dipole Antenna

The FDTD [40] method has been widely used to model lossy and dispersive materials, as well as antennas [41]. The FGCM method is validated against the FDTD method obtained with the commercial software SEMCAD X Matterhorn SOLUTIONS [42], while considering PEC and dielectric media. A dipole in the form of a 50×1.11 cm cylinder is placed 5 cm above a huge cube ($300 \times 300 \times 28$ cm) of PEC and lossy medium, as shown in Fig. 8. The medium has a relative permittivity of 5.54 and a conductivity of 0.0327 S/m. For the

TABLE IV
SEMCAD AND FGCM COMPUTATION TIMES

Operation	Time (s)
SEMCAD software	6.91
All radiation patterns	21.257
Γ_{TE} and Γ_{TM}	0.137
Update of Z^g when changing ground parameters while having patterns precalculated	1.67

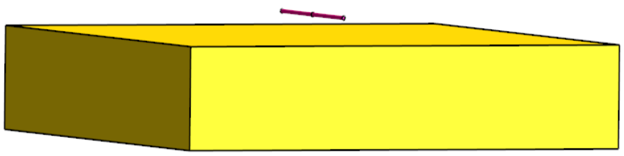

Fig. 8. Dipole in the presence of a layered medium; plot generated with SEMCAD.

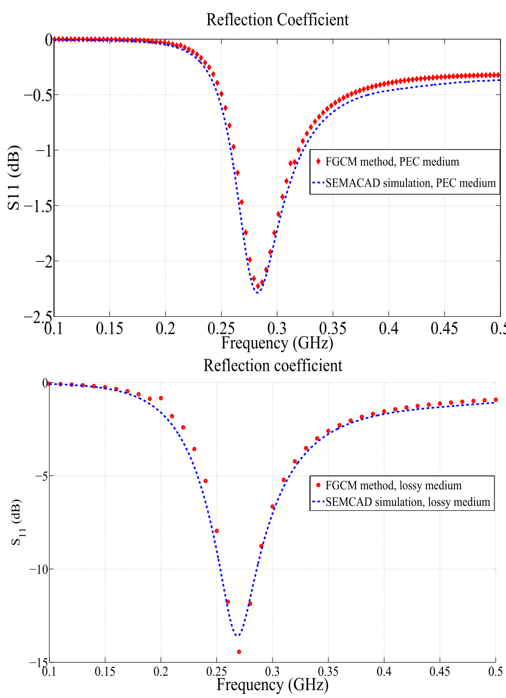

Fig. 9. Reflection coefficient comparison between FGCM method and SEMCAD simulation in the case of PEC and lossy media.

FGCM results, the dipole is discretized using the GMSH software into 1158 RWG BFs. The number of (k_x, k_y) grid points is set to $N_x = N_y = 35$. Fig. 9 shows a very good agreement between the FGCM method and SEMCAD simulation for both cases, i.e., PEC and lossy media, which validates the FGCM method over the FDTD technique.

Table IV compares the time needed for both methods for a single frequency.

IV. EXPERIMENTAL MEASUREMENT VALIDATION AND DISCUSSION

We show here the measured results for a single 3-D Vivaldi antenna prototype (Fig. 10). This antenna was initially

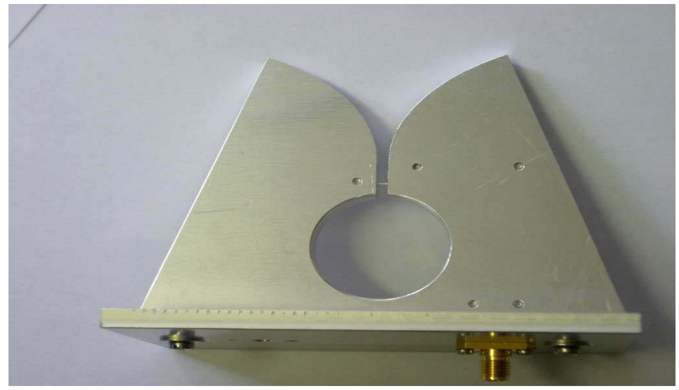

Fig. 10. 3-D Vivaldi antenna prototype.

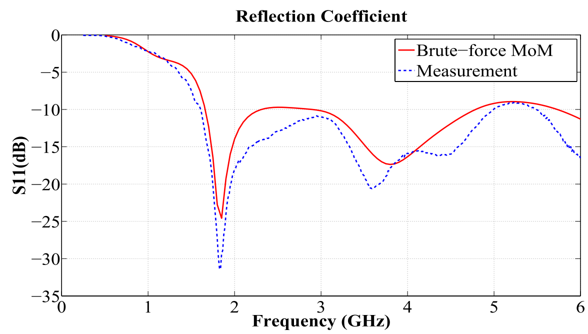

Fig. 11. Comparison of free-space reflection coefficient between the brute-force MoM and measurement for the 3-D single Vivaldi prototype.

designed as part of an antenna array for imaging applications [43]. The prototype operates from 1.5 to 6 GHz as shown in Fig. 11. Two cases of layered medium will be taken into consideration: PEC and lossy grounds. The measurements are recorded at different vertical distances between the antenna and the ground.

A. Experimental Validation in the Case of a Lossy Ground

Fig. 12 shows the measurement setup in the case of a lossy ground. The lossy medium consists of a stack of seven clay pavers; 280 mm thick with a metal plate underneath. The pavers have a relative permittivity of 4.8 ± 0.5 and a conductivity of 0.05 ± 0.015 S/m [44]. The Vivaldi antenna is placed at a distance of 0 mm (touching the pavers) and 23.5 mm above the lossy ground. As can be seen in Fig. 13,good agreement between the measured and FGCM results is achieved.

B. Experimental Validation in the Case of a PEC Ground

The pavers were replaced by a large metal plate (PEC) which is placed at 10.75 and 21.25 mm below the 3-D Vivaldi prototype. Fig. 14 shows a good level of agreement between the measurement and the FGCM results.

GPR data can be presented in time domain. The frequency domain signal obtained from the reflection coefficient is inverse Fourier transformed to obtain the time domain response. Fig. 15 shows the time domain response comparison for two cases: 1) the simulated difference between the free-space and a lossy medium of 7 clay pavers placed at 23.5 mm

Fig. 12. Experimental setup in the case of a lossy ground, showed with a stack of three clay pavers (the results presented in this paper use a thickness of seven pavers).

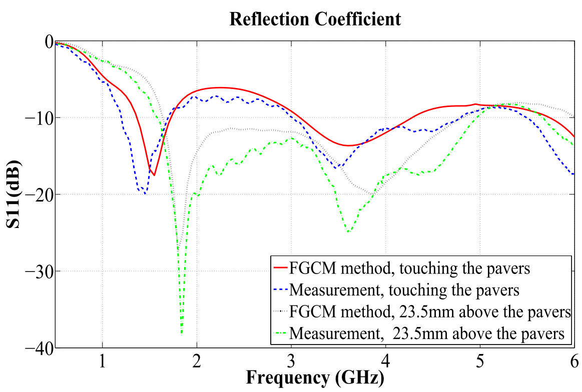

Fig. 13. Comparison of reflection coefficient between the FGCM method and measurement in the case of a lossy ground.

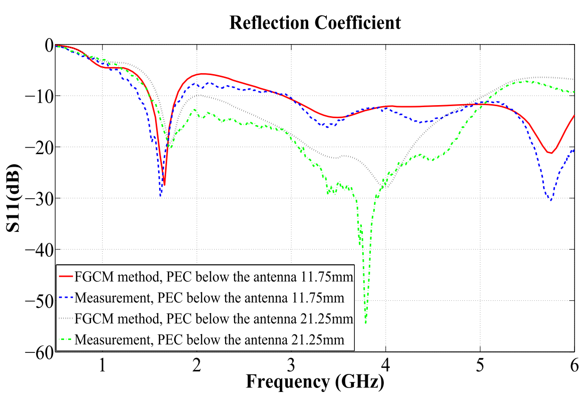

Fig. 14. Comparison of reflection coefficients between the FGCM method and measurement in the case of a PEC ground.

below the Vivaldi antenna with relative permittivity of 4.8±0.5 and conductivity of 0.05 ± 0.015 S/m, 280 mm thick with a metal plate underneath and 2) the measured difference for the same case as in 1). The antenna is fed with a unit voltage. The phase shift between the simulated and measured results has been corrected. This phase shift is due to the feed length difference between the GMSH model and the fabricated antenna. The cable length calculation is obtained from the free-space data. For simplicity, it is assumed that the coaxial cable in the Vivaldi antenna is lossless and leads to a phase factor of e^{jak_z}. A linear least squares method is used to find the value of a which minimizes the error between measurements

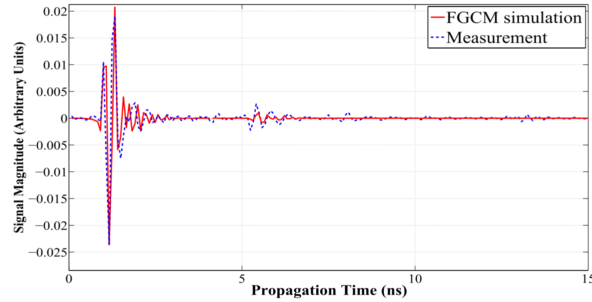

Fig. 15. Comparison of time domain response between the FGCM method and measurement in the case of a lossy medium.

TABLE V

LAYER THICKNESS OF SIMULATED AND MEASURED DATA

Operation	$d_n(mm)$	$\Delta n(\%)$
Simulated	295.2	5.1
Measured	290.7	3.6

and simulations. This allows to cater for the coaxial cable length. Fig. 15 shows a good matching between the simulated and measured results, where the first layer and the metal plate are well detected at the same time-domain peaks. The data obtained from Fig. 15 can be used to approximately calculate the layer thickness using the following equation:

$$d_n = \frac{(t_2 - t_1)\sqrt{\epsilon_r}}{2c} \tag{25}$$

where t_1 and t_2 are the timing of maxima corresponding to the first layer and the metal plate respectively, and c is the speed of light.

Table V shows the layer thickness calculated from the data obtained from the plot above, with the percent error in layer thickness Δn.

The precision of the simulation method may be evaluated by taking the maximum value of the absolute error between simulation and measurement at returns of particular interest and dividing by the maximum of the measured return with the antenna in free-space. For the return from the air/paver interface (large return at approximately 1.5 ns) this is -74dB, while it is -49 dB for the paver/metal interface (small return at approximately 6 ns). The loss in accuracy for the later return is probably due to difficulties in obtaining an accurate ground truth measurement of the paver's loss tangent. It should be noted that the free-space return has been removed from Fig. 15 to enable the later returns to be viewed clearly.

V. CONCLUSION

A novel fast method based on MoM solution of integral equation is proposed to add the contribution of ground on antennas. We named the method FGCM. The MoM impedance matrix is divided into two parts: the free-space matrix and the ground contribution matrix. The free-space matrix is obtained by conventional brute-force MoM solution. The ground contribution matrix is obtained by efficient multiplication of radiation patterns of the BFs/TFs and the reflection coefficient in the spectral domain. The spectral integration is carried out in 2-D spectral coordinates using the SDP. A minimum number of samples is achieved through compensation between aliasing and truncation errors. The physical parameters of the ground only appear through the reflection coefficient. This property allows for very fast update of the ground contribution matrix, while looping through soil parameters. The proposed method has been validated against the exact MoM solution in the case of a PEC ground. The FGCM method has also been validated against the commercial software IE3D in the case of a lossy multilayered ground, and SEMCAD (FDTD method) in the case of PEC and lossy mediums. Considering a 3-D wideband antenna, it has been shown that the FGCM method is 22 times faster than the MoM brute-force solution (1.5 s compared with 33.5 s) when changing the ground permittivity, conductivity, permeability, number of layers, layer thickness, and/or antenna height. Accurate experimental validation has been provided for antennas at a range of distances above both PEC and lossy dielectric grounds.

Acknowledgment

The authors would like to thank the anonymous reviewers for their precise comments on this paper.

References

[1] E. Pettinelli *et al.*, "A controlled experiment to investigate the correlation between early-time signal attributes of ground-coupled radar and soil dielectric properties," *J. Appl. Geophys.*, vol. 101, pp. 68–76, Feb. 2014.

[2] R. Solimene, A. D'Alterio, G. Gennarelli, and F. Soldovieri, "Estimation of soil permittivity in presence of antenna-soil interactions," *IEEE J. Sel. Topics Appl. Earth Observ. Remote Sens.*, vol. 7, no. 3, pp. 805–812, Mar. 2014.

[3] N. Diamanti, D. Redman, and A. Giannopoulos, "A study of GPR vertical crack responses in pavement using field data and numerical modelling," in *Proc. 13th Int. Conf. GPR*, Jun. 2010, pp. 1–6.

[4] M. R. Mahmoudzadeh, J. B. Got, S. Lambot, and C. Grégoire, "Road inspection using full-wave inversion of far-field ground-penetrating radar data," in *Proc. 7th Int. Workshop Adv. Ground Penetrating Radar (IWAGPR)*, Jul. 2013, pp. 1–6.

[5] L. Crocco, F. Soldovieri, N. J. Cassidy, and G. Prisco, "Early-stage leaking pipes GPR monitoring via microwave tomographic inversion," *J. Appl. Geophys.*, vol. 67, no. 4, pp. 270–277, Apr. 2009.

[6] A. Stampolidis, P. Soupios, F. Vallianatos, and G. N. Tsokas, "Detection of leaks in buried plastic water distribution pipes in urban places—A case study," in *Proc. 2nd Int. Workshop Adv. Ground Penetrating Radar*, Delft, The Netherlands, May 2003, pp. 120–124.

[7] S. Busch, J. van der Kruk, J. Bikowski, and H. Vereecken, "Quantitative conductivity and permittivity estimation using full-waveform inversion of on-ground GPR data," *Geophysics*, vol. 77, no. 6, pp. H79–H91, Oct. 2012.

[8] G. Hislop, "Permittivity estimation using coupling of commercial ground penetrating radars," *IEEE Trans. Geosci. Remote Sens.*, vol. 53, no. 8, pp. 4157–4164, Aug. 2015.

[9] S. Lambot, E. C. Slob, I. van den Bosch, B. Stockbroeckx, and M. Vanclooster, "Modeling of ground-penetrating Radar for accurate characterization of subsurface electric properties," *IEEE Trans. Geosci. Remote Sens.*, vol. 42, no. 11, pp. 2555–2568, Nov. 2004.

[10] D. Comite, A. Galli, S. E. Lauro, E. Mattei, and E. Pettinelli, "Analysis of GPR early-time signal features for the evaluation of soil permittivity through numerical and experimental surveys," *IEEE Trans. Geosci. Remote Sens.*, vol. 9, no. 1, pp. 178–187, Jan. 2016.

[11] C. A. Balanis, *Antenna Theory: Analysis and Design*, 3rd ed. New York, NY, USA: Wiley, May 2005, pp. 205–207.

[12] R. F. Harrington, *Field Computation by Moment Methods*. Piscataway, NJ, USA: Wiley, 1993.

[13] X. Millard and Q. H. Liu, "A fast volume integral equation solver for electromagnetic scattering from large inhomogeneous objects in planarly layered media," *IEEE Trans. Antennas Propag.*, vol. 51, no. 9, pp. 2393–2401, Sep. 2003.

[14] J. Yeo and R. Mittra, "An algorithm for interpolating the frequency variations of method-of-moments matrices arising in the analysis of planar microstrip structures," *IEEE Trans. Microw. Theory Techn.*, vol. 51, no. 3, pp. 1018–1025, Mar. 2003.

[15] J. K. Lee and J. A. Kong, "Dyadic Green's functions for layered anisotropic medium," *Electromagnetics*, vol. 3, no. 2, pp. 111–130, 1983.

[16] K. A. Michalski and D. Zheng, "Electromagnetic scattering and radiation by surfaces of arbitrary shape in layered media. I. Theory," *IEEE Trans. Antennas Propag.*, vol. 38, no. 3, pp. 335–344, Mar. 1990.

[17] A. Dreher, "A new approach to dyadic Green's function in spectral domain," *IEEE Trans. Antennas Propag.*, vol. 43, no. 11, pp. 1297–1302, Nov. 1995.

[18] W. C. Chew, J. S. Zhao, and T. J. Cui, "The layered medium Green's function—A new look," *Microw. Opt. Technol. Lett.*, vol. 31, no. 4, pp. 252–255, Nov. 2001.

[19] Y. Chen, S. Yang, S. He, and Z.-P. Nie, "Fast analysis of microstrip antennas over a frequency band using an accurate MoM matrix interpolation technique," *Prog. Electromagn. Res.*, vol. 109, pp. 301–324, Nov. 2010, ISSN 1070–4698.

[20] T. J. Cui and W. C. Chew, "Accurate model of arbitrary wire antennas in free space, above or inside ground," *IEEE Trans. Antennas Propag.*, vol. 48, no. 4, pp. 482–493, Apr. 2000.

[21] A. Giannopoulos, "Modelling ground penetrating radar by GprMax," *Construction Building Mater.*, vol. 19, no. 10, pp. 755–762, Dec. 2005.

[22] F. Keshmiri and C. Craeye, "Moment-method analysis of normal-to-body antennas using a Green's function approach," *IEEE Trans. Antennas Propag.*, vol. 60, no. 9, pp. 4259–4270, Sep. 2012.

[23] G. Hislop, N. A. Ozdemir, C. Craeye, and D. González-Ovejero, "MoM matrix generation based on frequency and material independent reactions (FMIR-MoM)," *IEEE Trans. Antennas Propag.*, vol. 60, no. 12, pp. 5777–5786, Dec. 2012.

[24] J. A. Kong, Ed., *Theory of Electromagnetic Waves*. Hoboken, NJ, USA: Wiley, 1975.

[25] E. Martini, C. Craeye, N. Ozdemir, and S. Maci, "Harmonics-based inhomogeneous plane-wave method (HIPW)," *IEEE Trans. Antennas Propag.*, vol. 63, no. 5, pp. 2331–2336, May 2015.

[26] G. Hislop, S. Lambot, C. Craeye, D. González-Ovejero, and R. Sarkis, "Antenna calibration for near-field problems with the method of moments," in *Proc. 5th Eur. Conf. Antennas Propag. (EUCAP)*, Rome, Italy, Apr. 2011, pp. 2004–2008.

[27] G. Hislop, C. Craeye, and D. González-Ovejero, "Antenna calibration for near-field material characterization," *IEEE Trans. Antennas Propag.*, vol. 64, no. 4, pp. 1364–1372, Apr. 2016.

[28] K. Alkhalifeh, N. Ozdemir, and C. Craeye, "Efficient simulation of coupled ground antennas," in *Proc. 9th Eur. Conf. Antennas Propag. (EUCAP)*, Lisbon, Portugal, Apr. 2015, pp. 1–4.

[29] D. M. Pozar and D. H. Schaubert, Eds., *Microstrip Antennas: The Analysis and Design of Microstrip Antennas and Arrays*. New York, NY, USA: IEEE Press, 1995.

[30] K. A. Michalski and J. R. Mosig, "Multilayered media Green's functions in integral equation formulations," *IEEE Trans. Antennas Propag.*, vol. 45, no. 3, pp. 508–519, Mar. 1997.

[31] W. B. Lu, T. J. Cui, X. X. Yin, Z. G. Qian, and W. Hong, "Fast algorithms for large-scale periodic structures using subentire domain basis functions," *IEEE Trans. Antennas Propag.*, vol. 53, no. 3, pp. 1154–1162, Mar. 2005.

[32] N. Yuan, T. S. Yeo, X.-C. Nie, and L. W. Li, "A fast analysis of scattering and radiation of large microstrip antenna arrays," *IEEE Trans. Antennas Propag.*, vol. 51, no. 9, pp. 2218–2226, Sep. 2003.

[33] H. Weyl, "Ausbreitung elektromagnetischer Wellen über einem ebenen Leiter," *Ann. Phys.*, vol. 365, no. 21, pp. 481–500, 1919.

[34] A. Fort, F. Keshmiri, G. R. Crusats, C. Craeye, and C. Oestges, "A body area propagation model derived from fundamental principles: Analytical analysis and comparison with measurements," *IEEE Trans. Antennas Propag.*, vol. 58, no. 2, pp. 503–514, Feb. 2010.

[35] S. N. Jha and C. Craeye, "Contour-FFT based spectral domain MBF analysis of large printed antenna arrays," *IEEE Trans. Antennas Propag.*, vol. 62, no. 11, pp. 5752–5764, Nov. 2014.

[36] E. Martini, S. Karki, C. Craeye, and S. Maci, "Error analysis of the harmonics-based plane wave method," in *Proc. Int. Conf. Electromagn. Adv. Appl. (ICEAA)*, Turin, Italy, Sep. 2015, pp. 1493–1495.

[37] S. M. Rao, D. R. Wilton, and A. W. Glisson, "Electromagnetic scattering by surfaces of arbitrary shape," *IEEE Trans. Antennas Propag.*, vol. 30, no. 3, pp. 409–418, May 1982.

[38] *GMSH: A Three-Dimensional Finite Element Mesh Generator With Built-In Pre- and Post-Processing Facilities*. accessed on Oct. 2016. [Online]. Available: http://gmsh.info/http://gmsh.info/

[39] Zeland Software Inc. *IE3D Electromagnetic Simulation and Optimization Package,Version 9.35*, Zeland Software Inc., Fremont, CA, USA, 2003.

[40] K. Yee, "Numerical solution of initial boundary value problems involving Maxwell's equations in isotropic media," *IEEE Trans. Antennas Propag.*, vol. AP-14, no. 3, pp. 302–307, May 1966.

[41] Y. El Hajibi and A. El Hamichi, "Simulation and numerical modeling of a rectangular patch antenna using finite difference time domain (FDTD) method," *J. Comput. Sci. Inf. Technol.*, vol. 2, no. 2, pp. 1–8, Jun. 2014.

[42] *SEMCAD X: EM/T Simulation Platform*. acceded on Oct. 2016. [Online]. Available: https://www.speag.com/

[43] K. Alkhalifeh, R. Sarkis, and C. Craeye, "Wheel-of-time array devoted to near-field imaging applications," in *Proc. Int. Conf. Electromagn. Adv. Appl. (ICEAA)*, Turin, Italy, Sep. 2013, pp. 1164–1167.

[44] G. Hislop, "Limitations of characterizing layered earth with off-ground GPR," *J. Geophys. Eng.*, vol. 13, no. 2, p. S1, Mar. 2016.

Khaldoun Alkhalifeh (M'16) was born in Aleppo, Syria, in 1981. He received the Diploma in electrical and electronic engineering from the Faculty of Electrical and Electronic Engineering, Aleppo University, Aleppo, in 2006, and the master's degree in microwave and telecommunication from the Université Catholique de Louvain, Louvain-la-Neuve, Belgium, in 2010, where he is currently pursuing the Ph.D. degree in antenna engineering.

From 2011 to 2016, he was a Research Assistant with the Antenna Research Group, Institute of Information and Communication Technologies, Electronics and Applied Mathematics, Université Catholique de Louvain. His current research interests include multiband antenna array design and analysis, ground penetrating radar applications, fast numerical methods for electromagnetic fields in finite periodic structures, and near-field imaging.

Greg Hislop (M'07–SM'14) was born in Australia in 1978. He received the bachelor's degree in electrical and electronic engineering and the Ph.D. degree (with his thesis focused on inverse scattering techniques for the imaging of shallowly buried objects with ground penetrating radar) from the Queensland University of Technology, Brisbane, QLD, Australia, in 2000 and 2006, respectively.

From 2005 to 2008, he was with the CSIRO ICT Center, Sydney, NSW, Australia, where he was involved in the application of phase retrieval techniques to terahertz imaging applications and the detection of faults in the trunks of plantation pines using radar. From 2009 to 2012, he was with the Université Catholique de Louvain, Louvain-la-Neuve, Belgium, where he was involved in the direction of arrival finding techniques, novel permittivity measurement methods, and integral equation electromagnetic simulation algorithms. From 2012 to 2015, he was a Research Scientist with CSIRO Energy Flagship, Brisbane, where he was involved in ground penetrating radar and electromagnetic inverse scattering/sensing techniques for application to intelligent mining. He is currently with Fugro-Roames, Brisbane, where he is a Research and Development Engineer.

Dr. Hislop was the Vice Chair in 2014 and the Chair of the IEEE's Queensland Antennas and Propagation and Microwave Theory and Techniques Joint Chapter in 2015.

Nilufer Aslihan Ozdemir (M'07) received the B.Sc. and M.Sc. degrees in electrical and electronics engineering from Middle East Technical University, Ankara, Turkey, in 1997 and 2000, respectively, and the Ph.D. degree in electrical and computer engineering from The Ohio State University, Columbus, OH, USA, in 2007.

In 2007, she was a Post-Doctoral Researcher with the Université Catholique de Louvain, Louvain-la-Neuve, Belgium. Her current research interests include the integral equation based numerical solution of electromagnetic scattering and radiation problems.

Christophe Craeye (M'98–SM'11) was born in Belgium in 1971. He received the Electrical Engineering and B.Phil. degrees and the Ph.D. degree in applied sciences from the Université Catholique de Louvain (UCL), Louvain-la-Neuve, Belgium, in 1994 and 1998, respectively.

From 1994 to 1999, he was a Teaching Assistant with UCL, where he carried out research on the radar signature of the sea surface perturbed by rain, in collaboration with NASA and ESA. He was with the University of Massachusetts at Amherst, Amherst, MA, USA, in 1999. From 1999 to 2001, he was a Post-Doctoral Researcher with the Eindhoven University of Technology, Eindhoven, The Netherlands. He was with the Netherlands Institute for Research in Astronomy, Dwingeloo, The Netherlands, in 2001, where his research was related to wideband phased arrays devoted to the square kilometer array radio telescope. In 2002, he started an antenna research activity at the Université Catholique de Louvain, where he is currently a Professor. He was with the Astrophysics and Detectors Group, University of Cambridge, Cambridge, U.K., in 2011. His research is funded by Région Wallonne, European Commission, ESA, FNRS, and UCL. His current research interests include finite antenna arrays, wideband antennas, small antennas, metamaterials, and numerical methods for fields in periodic media, with applications to communication and sensing systems.

Prof. Craeye was a recipient of the 2005-2008 Georges Vanderlinden Prize from the Belgian Royal Academy of Sciences in 2009. He was an Associate Editor of the IEEE TRANSACTIONS ON ANTENNAS AND PROPAGATION from 2004 to 2010. He is as an Associate Editor of the *IEEE Antennas and Wireless Propagation Letters*.